Cancer Cell International

RESEARCH

Open Access

Dysregulation of pseudouridylation in small RNAs contributes to papillary thyroid carcinoma metastasis

Xi Wang[1,2†], Hengyuan Gao[1,3†], Wenjun Pu[1], Zhipeng Zeng[1], Nan Xu[1], Xunpeng Luo[1], Donge Tang[1*] and Yong Dai[1,2,4,5*]

Abstract

Background Previous studies have indicated that ψ-modified small RNAs play crucial roles in tumor metastasis. However, the ψ-modified small RNAs during metastasis of PTC are still unclear.

Methods We compared the pseudouridine synthase 7 (PUS7) alteration between metastatic and non-metastatic PTCs, and investigated its correlation with clinicopathological features. Additionally, we employed a small RNA ψ modification microarray to examine the small RNA ψ modification profile in both metastatic and non-metastatic PTCs, as well as paired paracancerous tissues. The key molecule involved in ψ modification, pre-miR-8082, was identified and found to regulate the expression of CD47. Experiments in vitro were conducted to further investigate the function of PUS7 and CD47 in PTC.

Results Our results demonstrated that PUS7 was down-regulated in PTC and was closely associated with metastasis. Moreover, the ψ modification of pre-miR-8082 was found to be decreased, resulting in down-expression of pre-miR-8082 and miR-8082, leading to the loss of the inhibitory effect on CD47, thereby promoting tumor migration.

Conclusions Our study demonstrates that PUS7 promotes the inhibition of CD47 and inhibits metastasis of PTC cells by regulating the ψ modification of pre-miR-8082. These results suggest that PUS7 and ψ pre-miR-8082 may serve as potential targets and diagnostic markers for PTC metastasis.

Keywords Papillary thyroid cancer (PTC), Pseudouridylation (ψ), Small RNA, Tumor migration, pre-miRNA

†Xi Wang and Hengyuan Gao contributed equally to this work.

*Correspondence:
Donge Tang
donge66@126.com
Yong Dai
daiyong22@aust.edu.cn; daiyong22@aliyun.com
[1]The First Affiliated Hospital (Shenzhen People's Hospital), Southern University of Science and Technology, Shenzhen 518055, China
[2]The Fourth Clinical Medical College of Guangzhou, Shenzhen Traditional Chinese Medicine Hospital, University of Chinese Medicine, Shenzhen 518033, China
[3]Department of Thyroid Surgery, The First Affiliated Hospital of Jinan University, Guangzhou 510630, China
[4]The First Affiliated Hospital, School of Medicine, Anhui University of Science and Technology, Huainan 232001, China
[5]Peking University Shenzhen Hospital, Shenzhen 518036, China

Background

Thyroid cancer is currently the most prevalent endocrine malignancy [1]. The incidence of thyroid cancer, particularly papillary thyroid cancer (PTC), has significantly increased over the past few decades [2, 3]. Although PTC is generally considered to be a slow-growing tumor, some cancer cells can spread to the lymph nodes surrounding the thyroid gland [4]. PTCs without metastasis are generally considered low risk, as they have shown excellent patient outcomes. In cases of metastasis, a combination of surgery, radioactive iodine (RAI) ablation, and thyroid stimulating hormone (TSH) suppression are commonly

used. Unfortunately, a fraction of patients eventually develop resistance to RAI or succumb to the disease [5]. The presence of metastasis is a crucial factor in determining the prognosis, extent of surgery, and risk factors associated with high recurrence and low survival rates among PTC patients [6].

Preoperative ultrasound is a valuable tool for assessing metastasis in patients with PTC and can provide reliable information to assist in surgical management [7, 8]. However, accurately identifying lymph node metastasis through ultrasound remains challenging. While fine needle aspiration (FNA) can aid in ultrasound diagnosis [9], it is impractical to perform FNA on all lymph nodes before surgery. Consequently, there is an urgent need for a non-destructive and efficient method to predict metastasis risk in PTC patients and guide clinical diagnosis and treatment. It is crucial to investigate and comprehend the molecular mechanisms underlying the development and metastasis to facilitate accurate clinical diagnosis and treatment.

Recent studies have revealed that small RNA molecules, including pre-miRNA, miRNA, and tsRNA, play significant roles in post-transcriptional gene regulation. They are not merely intermediaries between DNA and protein or effector molecules [10]. Currently, more than 100 types of chemical modifications have been identified in cellular RNAs, such as pseudouridine (ψ), N1-methyladenosine (m1A), N6-methyladenosine (m6A), N7-methylguanosine (m7G), 5-methylcytosine (m5C), and uridylation [11]. Accumulated evidence suggests that abnormal expression of small RNA modifications is functionally linked to cancer hallmarks, including survival, proliferation, self-renewal, differentiation, stress adaption, invasion, and therapy resistance [12–15]. However, the specific small RNA modifications present in PTC and their role in tumorigenesis and progression remain unclear.

In this study, we utilized transcriptome data from 397 PTC samples obtained from the TCGA database, as well as small RNA modification microarray data from 9 PTC patients in our hospital. We observed a significant decrease in the expression of pseudouridine synthase 7 (PUS7) in PTC patients. Additionally, we found a significant alteration in small RNA ψ modification, particularly in patients with lymph node metastasis. Furthermore, our research revealed that PUS7 plays a role in CD47-mediated tumor cell proliferation and migration through its regulation of the ψ modification of pre-miR-8082. Overall, our study highlights the crucial role of small RNA ψ modification in the progression and metastasis of PTC, and its potential for aiding in the clinical diagnosis of PTC metastasis.

Methods

Patients and clinical samples

Paired samples of PTC tissues and paracancerous tissues were collected at Shenzhen People's Hospital. The PTC patients included in the study had not received any chemotherapy or radiotherapy before the tissue collection. Patients with infectious diseases such as chronic hepatitis B virus infection, autoimmune diseases like Hashimoto's thyroiditis, and primary hyperthyroidism were excluded from the study. The study ethics was approved by the ethics committees of the Shenzhen People's Hospital (LL-KY-2022091). The informed consents were collected from all the participants.

RNA extraction and quantitative real-time PCR

RNA was extracted from PTC and paracancerous tissues or cells using the TranZol Up Plus RNA Kit (TranGen Biotech, ER501), following the manufacturer's instructions. Subsequently, the RNA was reverse transcribed into cDNA using the EasyScript All-in-One First-Strand cDNA Synthesis SuperMix for qPCR (One-Step gDNA Removal) (TranGen Biotech, AE341). Quantitative real-time PCR was then conducted according to the manufacturer's instructions using PerfectStart Green qPCR SuperMix (TranGen Biotech, AQ601). The primers used in this study are listed in Supplemental Table 1.

Data source and description

We obtained the mRNA expression matrix file of TCGA-THCA which includes 397 samples with 712 normal, from the Genomic Data Commons Data Portal (https://www.ncbi.nlm.nih.gov/). Additionally, two mRNA expression datasets (GSE3678 and GSE129879) were retrieved from the GEO database (https://www.ncbi.nlm.nih.gov/geo/). These datasets consist of PTC and normal samples. To investigate protein expression data, we utilized the Human Protein Atlas (HPA) (https://www.proteinatlas.org/), a proteomics database that provides information on the organization and cellular distribution of human proteins. Specifically, we searched for PUS7, DNMT3B, and CD47 protein expression data in the HPA.

Arraystar human pseudouridine (ψ) small RNA modification microarray analysis

Nine pairs of PTCs and paracancerous tissue samples were selected for RNA extraction. The Arraystar Seq-StarTM poly(A) mRNA Isolation Kit (Aksomics, AS-MB-006-01/02) was used according to the manufacturer's instructions to obtain the small RNA. The quantity of RNA samples was determined using a NanoDrop ND-1000 spectrophotometer, and RNA integrity was assessed using a Bioanalyzer 2100 or gel electrophoresis. Each total RNA sample (1–5 μg) was immunoprecipitated with 4 μg of anti-pseudouridine antibody

(Diagenode, C15200247) and 1 mg of Protein G Dynabeads (Thermo Fisher, 11203D) in 500 μL of RIP buffer. The modified RNAs, referred to as 'IP', were extracted from the immunoprecipitated magnetic beads. The unmodified RNAs, known as 'Sup', were obtained from the supernatant. Arraystar's standard protocols were used to enzymatically label the 'IP' RNAs with Cy5, and the 'Sup' RNAs with Cy3 in separate reactions. The labeled RNAs were then combined and hybridized onto the Arraystar Human small RNA Modification Microarray (8×15 K). Finally, the array was scanned using an Agilent Scanner G2505C in two-color.

The acquired array images were analyzed using Agilent Feature Extraction software (version 11.0.1.1). The raw intensities of IP (immunoprecipitated, Cy5-labelled) and Sup (supernatant, Cy3-labelled) were normalized by taking the average of log2-scaled Spike-in RNA intensities. After normalization, the probe signals that had Present (P) or Marginal (M) QC flags in at least 4 out of 18 samples were retained. Multiple probes from the same small RNA (miRNA/tsRNA (tRF&tiRNA)/pre-miRNA) were combined into a single RNA level. The abundance of 'ψ' was analyzed based on the normalized intensities of Cy5-labelled IP (modified RNA). Differentially ψ-modified RNAs between two comparison groups were identified using fold change (FC) and statistical significance (*p*-value) thresholds. The ψ-modification patterns among samples were displayed using a hierarchical clustering heatmap created with R.

MeRIP-PCR

RNA was isolated from paired PTC and paracancerous tissue samples and diluted to a concentration of 2 μg/μl. The RNA was then fragmented at 65 ℃ for 5 min. A small aliquot of the fragmented RNA (5 μg) was reserved as the input sample for qPCR normalization. Dynabeads-sTM M-280 Sheep Anti-Mouse IgG (Invitrogen, 11201D) were used and washed twice with IP buffer (10 mM Tris pH_7.4, 250 mM NaCl, 0.1% NP-40) and then coupled with pseudouridine antibody (Diagenode C15200247) for 2 h at 4 ℃. Subsequently, the fragmented RNA and RNase inhibitor (Enzymatics, Y9240L) were added to the IP buffer. Samples were eluted with 200 μl Elution buffer (100 mM Tris pH 7.4, 1 mM EDTA, 0.05% SDS), 4 μl Proteinase K (Qiagen, 19131), and 2 μl RNase inhibitor for 1 h at 50 ℃ on a rotor. The supernatant was collected for RNA isolation.

For the RT reaction, 2 μl of RNA was used with either M-MuLV Reverse Transcriptase (Enzymatics, P7040L) for miRNA or SuperScriptTM III Reverse Transcriptase (Invitrogen) for pre-miRNA. The RT reactions were performed in the Gene Amp PCR System 9700 (Applied Biosystems). In the case of tsRNA, the RNA underwent pretreatment using the rtStar™ tRF&tiRNA Pretreatment Kit (Arraystar, AS-FS-005) to undergo acylation, 3'-cP removal, 5'-P addition, and demethylation. The rtStar™ First-Strand cDNA Synthesis Kit (3' and 5' adaptor) (Arraystar, AS-FS-003) instructions were followed, including ligation of the 3' splice, reverse transcription primer hybridization, and ligation of the 5' for cDNA synthesis for tsRNA. Each cDNA sample was configured separately with a realtime PCR reaction system. The prepared 384-PCR plate was then placed on a QuantStudio5 Real-time PCR System (Applied Biosystems) for PCR reactions. The resulting data were analyzed using the $2^{-\triangle\triangle Ct}$ method to calculate the percentage of input (%Input) for each MeRIP fraction. The %Input value was determined using the formula %Input=2^{-Ct}MeRIP/(2^{-Ct}MeRIP+2^{-Ct}Supernatant)*Fd*100%. The primers used are listed in Supplemental Table 1.

Cell culture and transfection

The human PTC cell lines B-CPAP and human normal thyroid cells Nthy-ori 3−1 were obtained from Fenghui Biotechnology Co., Ltd (Hunan, PR China). The cell lines were cultured in RPMI-1640 medium (Gibco, C11875500BT) supplemented with 10% fetal bovine serum (ExCell Bio, FSP500), 100 μg/mL penicillin, and 0.1 mg/mL streptomycin. The cells were maintained in a humidified atmosphere at 37 °C with 5% CO_2.

For the transfection experiments, B-CPAP and Nthy-ori 3−1 cells were divided into different groups. These groups included the si-NC control group (transfected with si-NC control), the mimic NC control group (transfected with mimic NC), the si-PUS7 or si-CD47 group (transfected with si-PUS7 or si-CD47), and the si-PUS7+miR-8082 group (transfected with both si-PUS7 and miR-8082 mimic). The si-PUS7 (5'-GGAAGAAGAGGAGGAAGAU-3') or si-CD47 (5'-GGAUCCAGUCACCUCUGAATT-3') and si-NC (5'-UUCUCCGAACGUGUCACGUTT-3') control were obtained from Sangon Biotech (Shanghai, PR China). The microRNA mimic (5'- UGAUGGAGCUGGGAAUACUCUG-3') and mimic NC (5'- UUGUACUACACAAAAGUACUG-3') were also obtained from Sangon Biotech (Shanghai, PR China). B-CPAP and Nthy-ori 3−1 cells were transfected at ~70–80% confluency with siRNA or microRNA mimic using Lipofectamine 3000 (Invitrogen, L3000-015) following the manufacturer's instructions.

MTT assay

Cells were seeded into 96-well plates at a density of 2×10^3 cells per well, 24 h after transfection with si-RNA or si-NC. The plates were then incubated at 37 °C with 5% CO_2 for 48 h. Next, 10 μl of MTT solution (Sigma-Aldrich, M5655-1G) was added to each well, followed by an additional 4 h of incubation. After dissolving the intracellular formazan crystals in DMSO (150 μL per

well; Sigma-Aldrich, D8418) for 20 min, the absorbance at 490 nm was measured using an Emax precision microplate reader (BioTek, PR China). The experiments were repeated at least three times, with 5–6 wells being set up each time.

Cell cycle analysis

Cell digestion was carried out using trypsin, followed by centrifugation and removal of the supernatant. The cells were then resuspended in ice-cold PBS and underwent repeated washing. To ensure proper fixation, single cell suspensions were prepared by adding ice-cold 70% ethanol solution to the cell and incubating it for more than 24 h at 4 °C. After centrifugation and washing with ice-cold PBS, the samples were stained with PI staining solution (MedChemExpress, HY-K1071-50T). Flow cytometry analysis was conducted using a BD FACSCanto II flow cytometer (BD Biosciences, US) and the results were analyzed using FlowJo X 10.0.7 (BD, US). The experiments were repeated at least three times.

Measurement of cell apoptosis

The Annexin V-FITC/PI apoptosis kit (MULTI SCIENCES, AP101-100) was utilized to evaluate apoptosis in B-CPAP and Nthy ori 3−1 cells. After treatment, the cells were collected and washed with ice-cold PBS twice. They were then resuspended in binding buffer and harvested into centrifuge tubes. Subsequently, the cells were incubated with Annexin V/PI in the dark for 15 min. The apoptotic cells were quantified using a BD FACSCanto II flow cytometer (BD Biosciences, US). Cells transfected with a scrambled si-RNA were used as the negative control. Early phase apoptotic cells were categorized as Annexin V+/PI- and late phase apoptotic cells as Annexin V+/PI+. The results of the experiments were detected and analyzed using FlowJo X 10.0.7 (BD, US) and the BD FACSCanto II flow cytometer. The experiments were repeated at least three times.

Cell migration assay

A Wound Healing assay was performed to investigate cancer cell migration. B-CPAP cells were transfected with si-RNA or si-NC and then seeded into 12-well plates and grew until they reached 80% confluence. To create wounds, the monolayer cells were scraped using a 200 µl pipette tip, and any non-adherent cells were removed by washing with the medium. After 48 h, the treated and control cells were examined, and migration images were captured using a 10x objective in phase-contrast microscopy. The rate at which cells moved towards the scratched area was used to determine cell migration. The size of the scratched area was quantified using ImageJ™ software.

Statistical analysis

The experiments were repeated at least three times. Statistical data were analyzed using GraphPad Prism 7.0 software and presented as the Mean ± SD of results from three independent experiments. The statistical analyses included the Student's *t*-test and one-way ANOVA. A p-value < 0.05 was considered statistically significant.

Results

PUS7 was decreased in PTCs and associated with metastatic

To investigate the potential role of small RNA modification in PTCs, we initially analyzed the expression of six common modifying enzymes using The Cancer Genome Atlas Thyroid Carcinoma (TCGA-THCA) dataset. Our findings indicated a significant decrease in the expression of five out of six RNA modifying enzymes in PTC tumors compared to normal tissues (Fig. 1A). Specifically, the core components of the RNA m5C methyltransferases complex, namely DNMT1, DNMT3A, and DNMT3B, along with the key enzyme of m6A, METTL3, and the pseudouridine synthase 7 (PUS7), exhibited significant downregulation in PTC tumors. Further analysis of the expression in non-metastatic and metastatic PTCs revealed that DNMT3B, METTL1, and PUS7 were significantly underexpressed in the metastatic PTCs (Fig. 1B). DNMT3B and PUS7 showed a lower level of expression in non-metastatic PTCs and exhibited a further decrease in metastatic PTCs, suggesting a correlation with PTC progression. These findings highlighted the important physiological functions of DNMT3B and PUS7 in PTCs. To confirm the specific link between PUS7, which mediates small RNA ψ modification, or DNMT3B, which mediates small RNA m5C modification, and PTCs, we analyzed the correlation of DNMT3B or PUS7 expression with clinical characteristics (Fig. 1C and D). The distribution of the pN stage and pTNM stage between the PUS7-high and PUS7-low groups showed a significant difference. The qPCR assay demonstrated that PUS7 was downregulated in PTC tissues and was significantly downregulated in metastasis compared to non-metastatic PTCs (Fig. 1E). Immunohistochemistry staining revealed a lower expression of PUS7 in PTCs compared to normal tissues (Fig. 1F). Additionally, we also conducted a qPCR assay and found no significant alterations in DNMT3B expression between normal and tumor tissues, as well as between non-metastatic and metastatic tumors (Figure S1E and S1F). These findings suggested that PUS7, which mediates small RNA ψ modification, could play an important role in the progression of PTCs.

Pus7 impaired PTC progression

To investigate the functions of PUS7 in PTC, we conducted a comparative analysis of differentially expressed

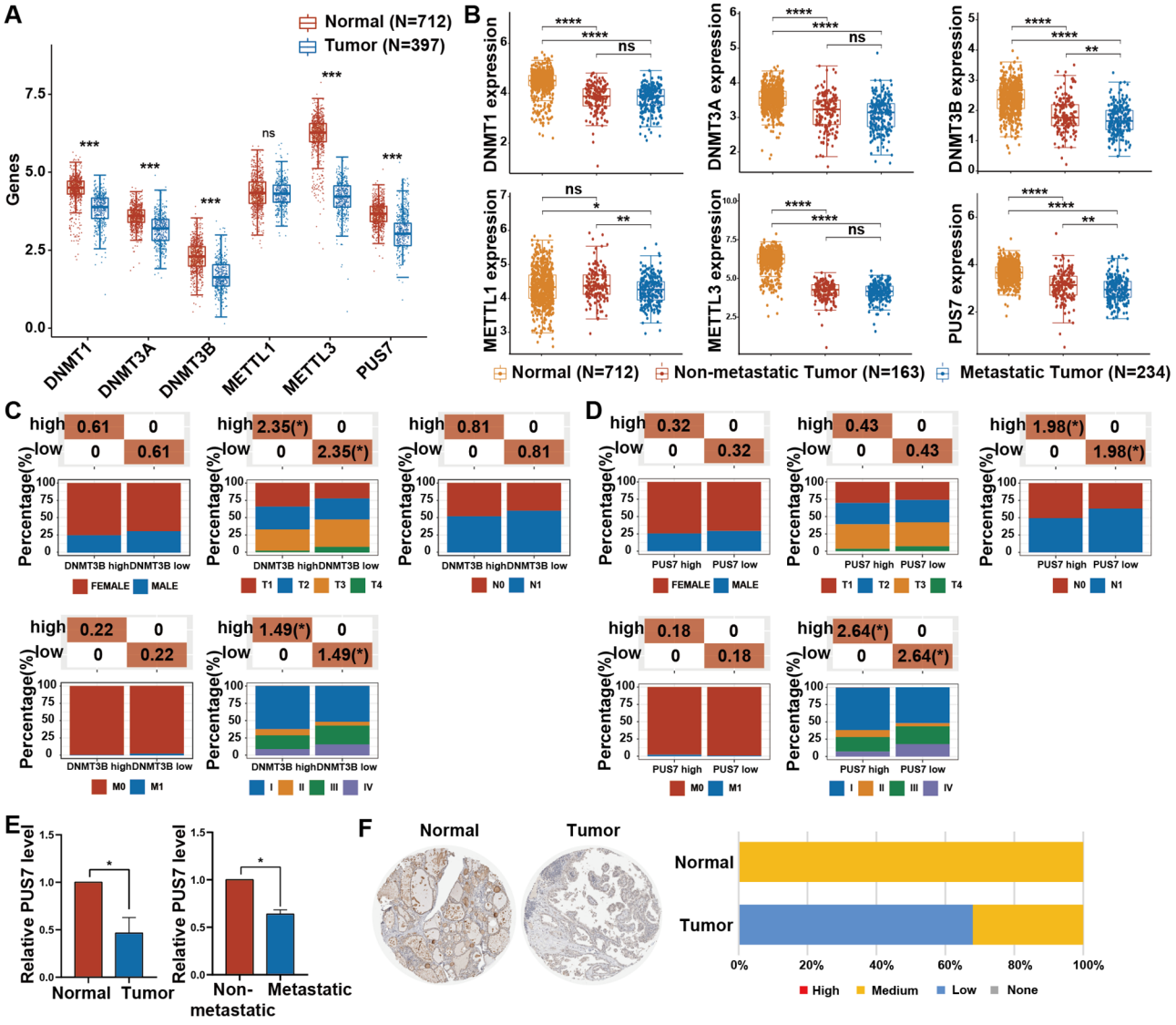

Fig. 1 Decreased expression of the PUS7 in PTC tissues. **A**. Comparison of the relative expression of RNA modification enzymes in PTCs (blue box) and normal tissues in TCGA-THCA. **B**. Comparison of the expression of RNA modification enzymes between non-metastatic PTCs (red box), metastatic PTCs (blue box), and normal tissues (yellow box) in TCGA-THCA. **C-D**. Correlation analysis between the expression of DNMT3B (**C**) or PUS7 (**D**) and clinical characteristics (gender, pT stages, pN stages, pM stages, and pTNM stages). The high group represents gene expression above the median expression levels, while the low group represents gene expression below the median expression levels. **E-F**. Quantitative analysis of PUS7 levels by qPCR (**E**) and IHC staining (**F**, data from HPA). Data are presented as Mean ± SD, *$p < 0.05$, **$p < 0.01$, ***$p < 0.001$, ****$p < 0.0001$

genes (DEGs) between PTCs with high PUS7 expression and low PUS7 expression. We performed an enrichment analysis of the DEGs for KEGG pathways and GO terms, as shown in Figure S2. The KEGG enrichment data revealed that PUS7 may have an impact on multiple pathways, including the TGF-beta signaling pathway, relaxin signaling pathway, platelet activation, and focal adhesion. These pathways have been previously reported to be cancer related, indicating the potential modulatory roles of PUS7 in PTC tumorigenesis. Subsequently, we utilized si-PUS7 to knock down PUS7 in B-CPAP, a commonly used PTC cell line (Fig. 2A). Our findings demonstrated that the loss of PUS7 leads to accelerated cell growth in B-CPAP cells (Fig. 2B). Furthermore, cell cycle analysis using PI staining revealed a significant increase in the proportion of cells arrested in the G2/M phase in PUS7 knockdown B-CPAP cells (Fig. 2C). Additionally, Annexin V/propidium iodide (PI) staining demonstrated that the depletion of PUS7 also resulted in decreased cell apoptosis in PTCs (Fig. 2D). Moreover, the knockdown of PUS7 enhanced the migratory abilities of PTC cells (Fig. 2E). Overall, our in vitro results unveiled a crucial role of PUS7 in the regulation of PTC progression.

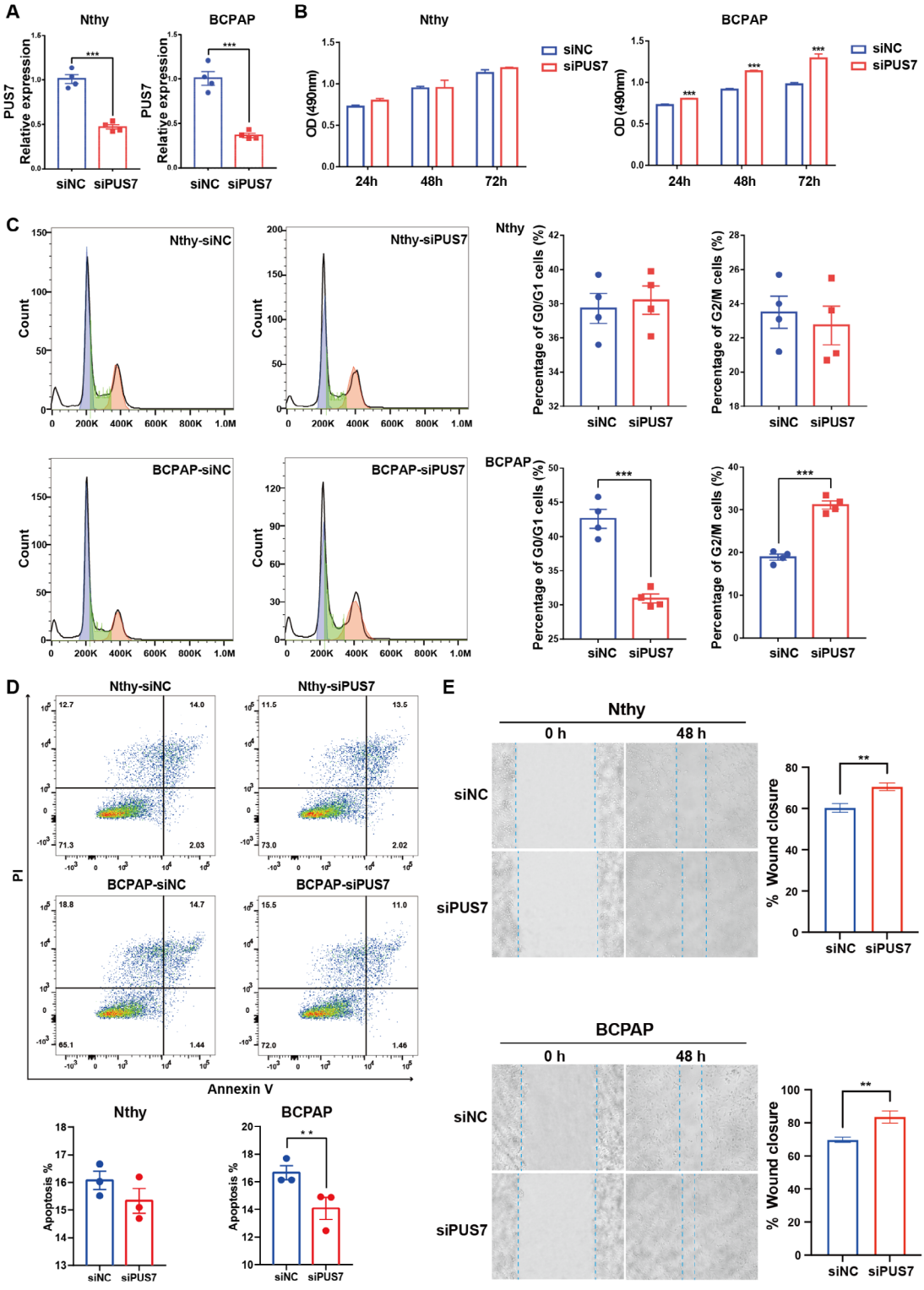

Fig. 2 PUS7 impairs PTC progression in vitro. **A**. qPCR confirmation of PUS7 depletion using siPUS7 in B-CPAP and Nthy ori 3 – 1 cells. **B**. MTT assay of PUS7-depleted B-CPAP cells or Nthy ori 3 – 1 cells. **C**. PI staining of PUS7-depleted B-CPAP cells or Nthy ori 3 – 1 cells. Left panels: representative images. Right panels: quantification data. **D**. Annexin V/PI analysis of PUS7-depleted B-CPAP cells or Nthy ori 3 – 1 cells. Top: representative images. Bottom: quantification data. **E**. Wound Healing assay of PUS7-depleted B-CPAP cells or Nthy ori 3 – 1 cells. Left panels: representative images. Right panels: quantification data. Data are presented as mean ± SD. $**p < 0.01$, $***p < 0.001$. siNC, negative control siRNA. All in vitro assays were biologically repeated three times

PUS7 regulated ψ modification of miRNA, pre-miRNA, and tsRNA in PTCs

To investigate the role of PUS7 in regulating PTC progression, we conducted a study using 9 pairs of PTCs and paracancerous tissues. We focused on assessing small RNA ψ modification and analyzed the clinical indexes of the 9 patients, with 4 patients showing lymphatic metastasis (Fig. 3A, Supplementary Table 2). Our analysis identified a total of 2047 miRNAs, 539 pre-miRNAs, and 3344 tsRNAs. Among these, 102 miRNAs, 154 pre-miRNAs, and 221 tsRNAs showed differential ψ modification in PTCs ($p<0.05$ & fold-change>=1.5 or <=1/1.5, Fig. 3D-F). Notably, the proportion of modified pre-miRNAs was significantly higher than that of the other two types of small RNAs, accounting for 28.57% of the total. The differential modification of small RNAs was visualized using volcanos and heat maps. Our data revealed significant differences between non-metastatic and metastatic PTCs, particularly in terms of differentially modified pre-miRNAs. We further compared the modification of miRNA, pre-miRNA, and tsRNA in non-metastatic and metastatic PTCs, and the heatmap highlighted the differences (Fig. 3G, Figure S3). Additionally, we observed a significant downregulation of ψ modification in pre-miR-8082 compared to paracancerous tissues, with even lower levels in metastatic PTCs (Fig. 3H), consistent with the expression of PUS7 in PTCs. Overall, our findings suggested that ψ modification of pre-miR-8082 may play a regulatory role in PTC progression and metastasis.

ψ modification of pre-miR-8082 regulated the expression of CD47 in PTC

Pre-miR-8082 is the precursor of miR-8082. The lower ψ modification of pre-miR-8082 has been found to decrease the expression of miR-8082 in PTCs, particularly in metastatic PTCs (Fig. 4A and B). To identify the downstream mRNA targets of PUS7-mediated pre-miR-8082 ψ modification, we utilized the TargetScan and miRDB databases to predict the target genes of miR-8082 (Supplementary Table 3). By incorporating data from the GEO database (GSE3678 and GSE129879), we identified seven target genes (SOX4, CD47, SLC16A7, PSMB2, CD74, S100B, and GAS7) that showed differential expression in PTCs (Fig. 4C and D). The expression of these seven genes in PTCs was further validated by TCGA, and our results demonstrated that CD47 expression was significantly upregulated in PTC, particularly in metastatic tumors (Fig. 4E and F). These findings were confirmed through IHC experiments (Fig. 4G). Subsequently, we analyzed the relationship between CD47 expression and metastasis, revealing that tumors with high CD47 expression were more prone to metastasize (Fig. 4H). Rescue experiments were conducted to validate the regulatory effect of PUS7 and miR-8082 on CD47. Knocking down CD47 using si-CD47 in B-CPAP cells (Fig. 5A) showed that loss of PUS7 inhibited cell growth (Fig. 5B). Cell cycle analysis indicated a significant decrease in the proportion of cells arrested in the G2/M phase in CD47 knockdown B-CPAP cells (Fig. 5C). Additionally, Annexin V/propidium iodide (PI) staining revealed that depletion of CD47 led to increased cell apoptosis in PTCs (Fig. 5D). Furthermore, the knockdown of CD47 inhibited the migratory abilities of PTC cells (Fig. 5E). Overall, these data suggested that decreased ψ modification of pre-miR-8082 selectively promotes CD47 expression in PTCs.

CD47 affected tumor proliferation and migration by regulating cell adhesion

CD47 is frequently found to be overexpressed in tumors and can transmit inhibitory signals to macrophages through signal regulatory protein α (SIPRα), thereby suppressing macrophage phagocytosis of tumor cells and facilitating tumor immune evasion. We further investigated the infiltration of M1-macrophages in PTCs and observed a reduction in infiltration in PTCs with high CD47 expression (Figure S4A). However, there was no significant correlation between CD47 and macrophage infiltration (Figure S4B). This suggests that CD47 may have a regulatory role in PTCs independent of macrophages. To examine the functions of CD47 in PTCs, we compared the differentially expressed genes (DEGs) between PTCs with high CD47 expression and low CD47 expression and performed enrichment analysis for KEGG pathways (Fig. 6A and B). The KEGG enrichment data revealed that CD47 might influence multiple pathways, including adhesion junction and focal adhesion. We validated the DEGs in the adhesion junction pathway using qPCR in vitro, as this pathway had the highest enrichment score, and the results were depicted in Fig. 6C. In conclusion, our findings confirmed that CD47 may enhance tumor cell proliferation and migration by regulating the adhesion function of tumor cells.

Discussion

Metastasis is a crucial determinant of the prognosis and surgical approach for PTC. It is also a significant risk factor for the high recurrence rate and low survival rate of patients. Therefore, understanding the molecular mechanism of PTC occurrence and metastasis holds great importance in the clinical diagnosis and treatment of PTC metastasis. Small RNAs, a heterogeneous group of noncoding RNAs, have emerged as promising molecules for risk stratification of cancer patients and have been found to play a role in tumorigenesis. In recent years, there has been an expansion in the field of small RNA research, with a greater focus on studying their expression. Small RNAs are involved in crucial cellular processes that are often dysregulated in cancer, and their

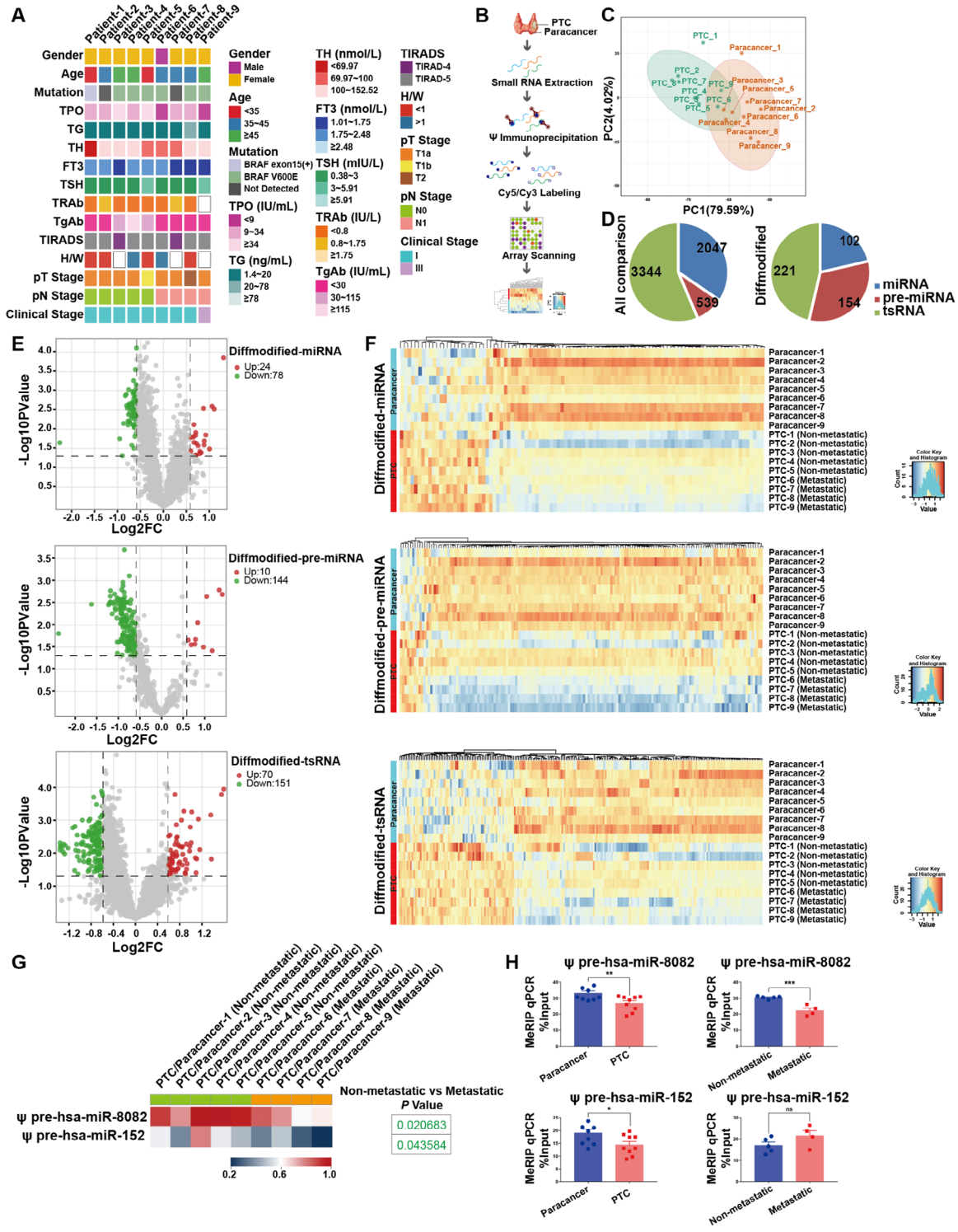

Fig. 3 Effects of PUS7 on miRNA, pre-miRNA and tsRNA ψ modification. **A**. Clinical index of 9 paired PTCs and paracancerousous tissues. **B**. Workflow of Arraystar Human Pseudouridine (ψ) small RNA modification microarray analysis. **C**. PCA plot comparing the PTC group and the paracancer group. **D**. The number of miRNAs, pre-miRNAs, and tsRNAs identified in PTCs and paracancerous tissues (Left), and the number of differentially modified miRNAs, pre-miRNAs, and tsRNAs found in PTCs (Right). **E-F**. Volcano plot (**E**) and heatmap (**F**) of diff-modified miRNAs, pre-miRNAs, and tsRNAs. **G**. The top two differentially modified pre-miRNAs. **H**. MeRIP-qPCR validation of ψ modification of pre-miR-8082 and pre-miR-152. Data are presented as mean ± SD. $*p < 0.05$, $**p < 0.01$, $***p < 0.001$

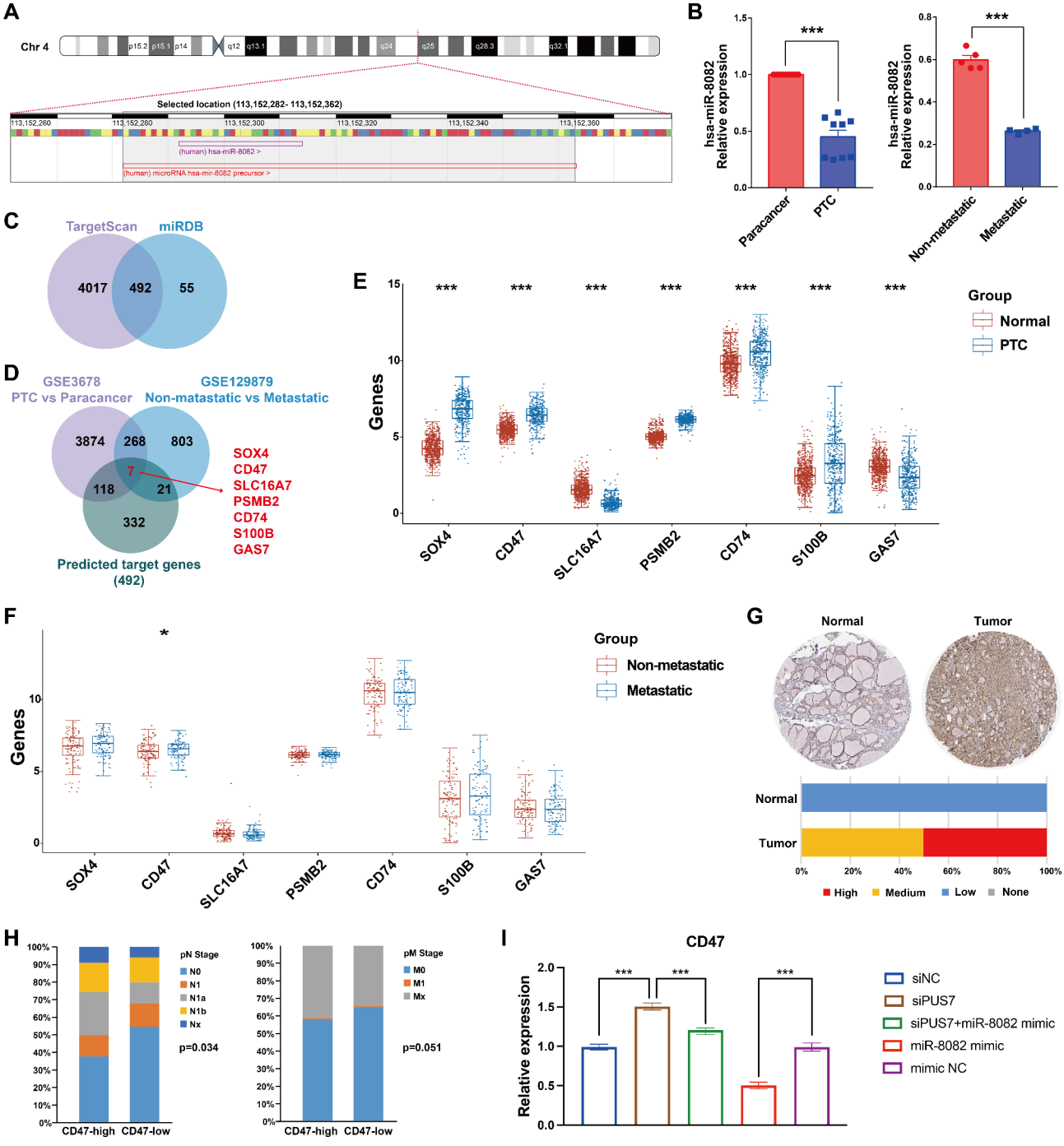

Fig. 4 ψ modification of pre-miR-8082 promotes the expression of CD47 in PTC. **A**. Localization of pre-miR-8082 on the chromosome. **B**. Expression of miR-8082 in paired PTC and paracancerous tissues. **C**. TargetScan and miRDB databases were used to predict the target genes of miR-8082. **D**. Venn diagram of the intersection of differentially expressed genes and predicted target genes in the GSE3678 and GSE129879 datasets. **E-F**. Validation of the seven differentially expressed target genes by TCGA database. **G**. Quantitative analysis of CD47 levels by IHC staining (data from HPA). **H**. Proportion of lymphatic metastases and distant metastases in PTCs with high or low CD47 expression. **I**. qPCR analysis of si-PUS7, si-PUS7 + miR-8082 mimic, and miR-8082 mimic transfected B-CPAP cells. Data are presented as mean ± SD. $*p < 0.05$, $***p < 0.001$

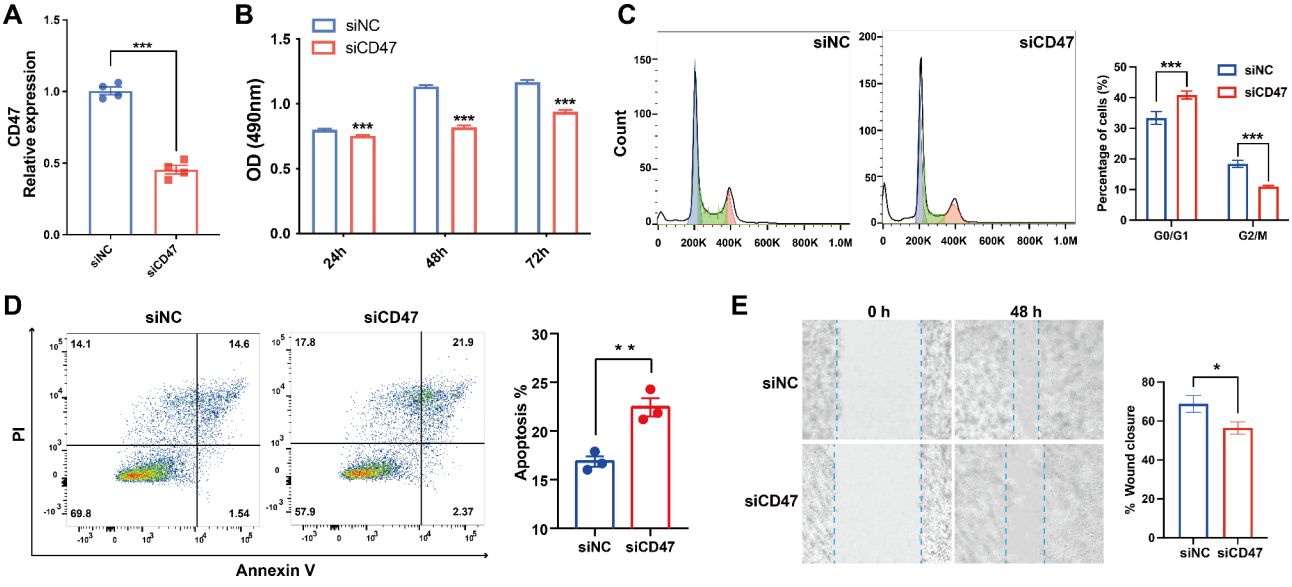

Fig. 5 CD47 accelerates PTC progression in vitro. **A**. qPCR analysis of CD47 in si-CD47 transfected B-CPAP cells. **B**. MTT assay of CD47-depleted and control B-CPAP cells. **C**. PI staining of CD47-depleted and control B-CPAP cells. Left panels: representative images. Right panels: quantification data. **D**. Annexin V/PI analysis of CD47-depleted and control B-CPAP cells. Left panels: representative images. Right panels: quantification data. **E**. Wound Healing assay of CD47-depleted and control B-CPAP cells. Left panels: representative images. Right panels: quantification data. Data are presented as mean ± SD. $^{**}p < 0.01$, $^{***}p < 0.001$. siNC, negative control siRNA

impact on tumorigenesis can be reflected [16]. Various classes of small RNAs have demonstrated prognostic value and functional roles in cancer.

Pseudouridine (ψ) is the C5 glycosidic isomer of uracil and was the first post-transcriptional modification to be discovered. It is also one of the most abundant RNA modifications [17]. Ψ can occur through two different mechanisms: RNA-independent and RNA-dependent ψ [18]. RNA-independent ψ is catalyzed by the pseudouridine synthase (PUS), which recognizes the substrate and performs catalysis without the need for an RNA template strand. From a clinical perspective, PUSs or ψ can serve as potential targets for anticancer therapy and biomarkers. For instance, high levels of ψ have been found in the urine of patients with colon, prostate, or ovarian cancer, in the plasma of ovarian cancer patients, and in the salivary metabolites of patients with oral squamous cell carcinoma [19–21]. This suggests that ψ could be a promising biomarker for non-invasive early detection of cancer through body fluid biopsies. Although abnormal expression of several ψ synthases has been observed in cancer, it remains unclear whether they could be effective targets for diagnosis and therapy. Therefore, further research is necessary to investigate the specific role of ψ synthases in tumor initiation, growth, and metastasis.

To investigate the changes in the expression of ψ and its regulatory enzyme PUS7 in PTC tissues, we analyzed the differential expression of PUS7 between PTC and paracancerous tissues and metastatic and non-metastatic PTCs. Our findings confirm that PUS7 regulates the proliferation and migration of tumor cells in PTC. Our results demonstrate a significant downregulation of PUS7 expression in PTC, with a more pronounced downregulation in metastatic PTC. ψ, a post-transcriptional RNA modification, plays a precise role in coordinating gene expression and biological processes. Existing literature suggests that ψ is critically involved in the early development of several organisms, contributing to cell fate specification and physiology [22]. The coordinated effects of different classes of modified RNAs and their regulator proteins generate a novel code that orchestrates gene expression during cell fate determination. In PTC, the modification level of small RNA ψ, regulated by PUS7, was significantly altered. This alteration was observed in approximately 5% of miRNA, 29% of pre-miRNA, and 7% of tsRNA. Surprisingly, nearly 1/4 of the pre-miRNAs were differentially modified. Importantly, dysregulation of pre-miRNA processing leads to aberrant miRNA expression in cancer [23]. RNA modifications play crucial roles in RNA metabolism and modulate miRNA biogenesis and function [24]. The RNA methyltransferase BCDIN3D has been reported to inhibit miRNA maturation through phospho-dimethylation of the 5' ends of pre-miRNAs [25]. However, our finding is the first report on ψ modification of pre-miRNA and its role in the PTC.

The ψ modification level of the pre-miR-8082 exhibits the most significant difference. Pre-miR-8082 is an RNA precursor transcribed from the genome, which undergoes multiple intracellular processing steps to generate mature microRNA and is used to regulate gene expression. PUS7

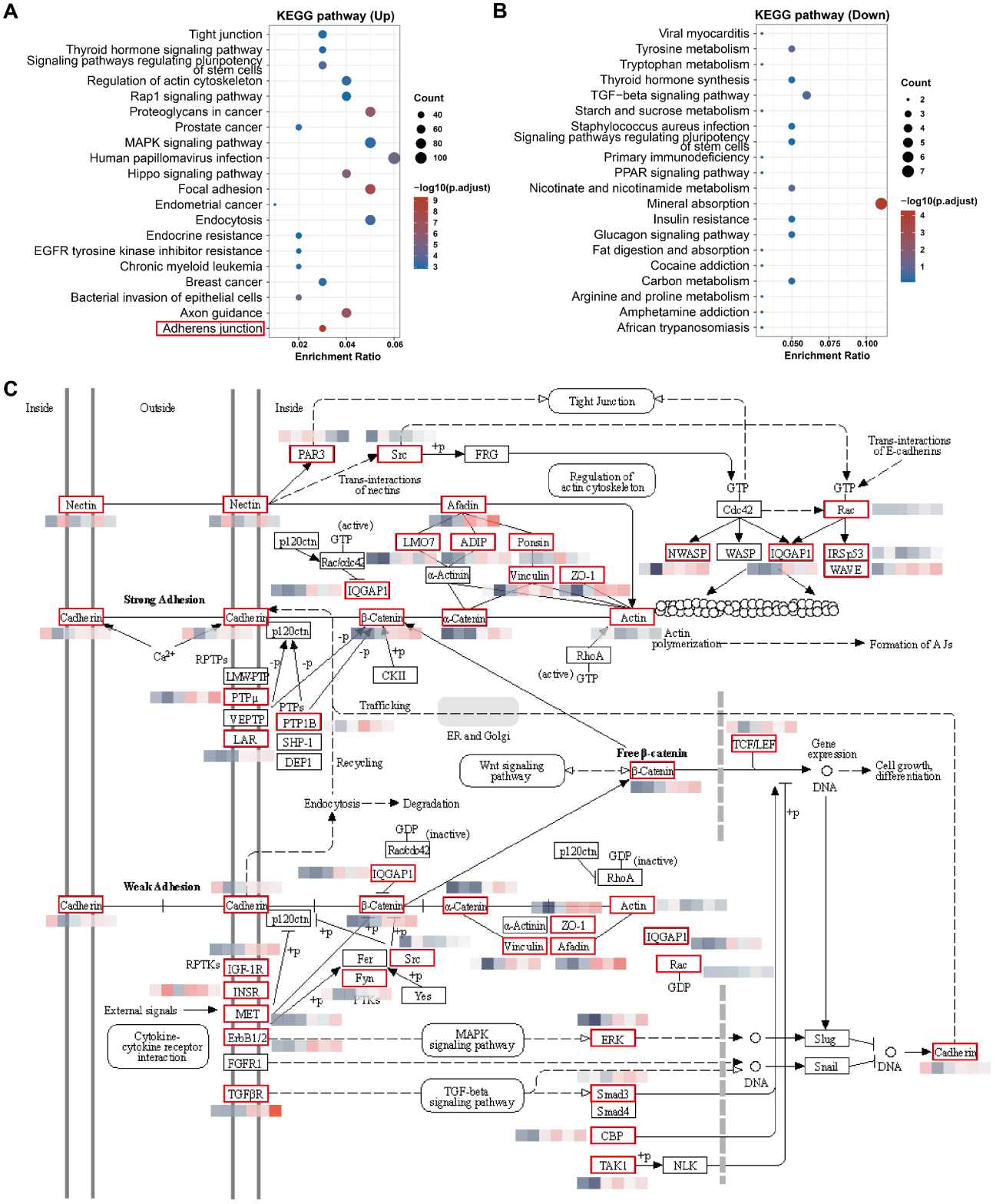

Fig. 6 CD47 affects the adhesion junction of tumor cells. **A-B**. Enrichment of KEGG pathways in the CD47-high vs. CD47-low group of PTCs. The high group represents genes with expression levels above the median, while the low group represents genes with expression levels below the median. **C**. qPCR assays for the differentially expressed genes (DEGs) of the adhesion junction pathway in si-CD47 transfected B-CPAP cells. The genes highlighted in red boxes indicate the DEGs of the adhesion junction pathway. The left 3 pixels beside the gene name represent si-CD47 transfected PTC cells, while the right 3 pixels represent si-NC transfected PTC cells. Blue and red colors indicate relatively low and high expression, respectively

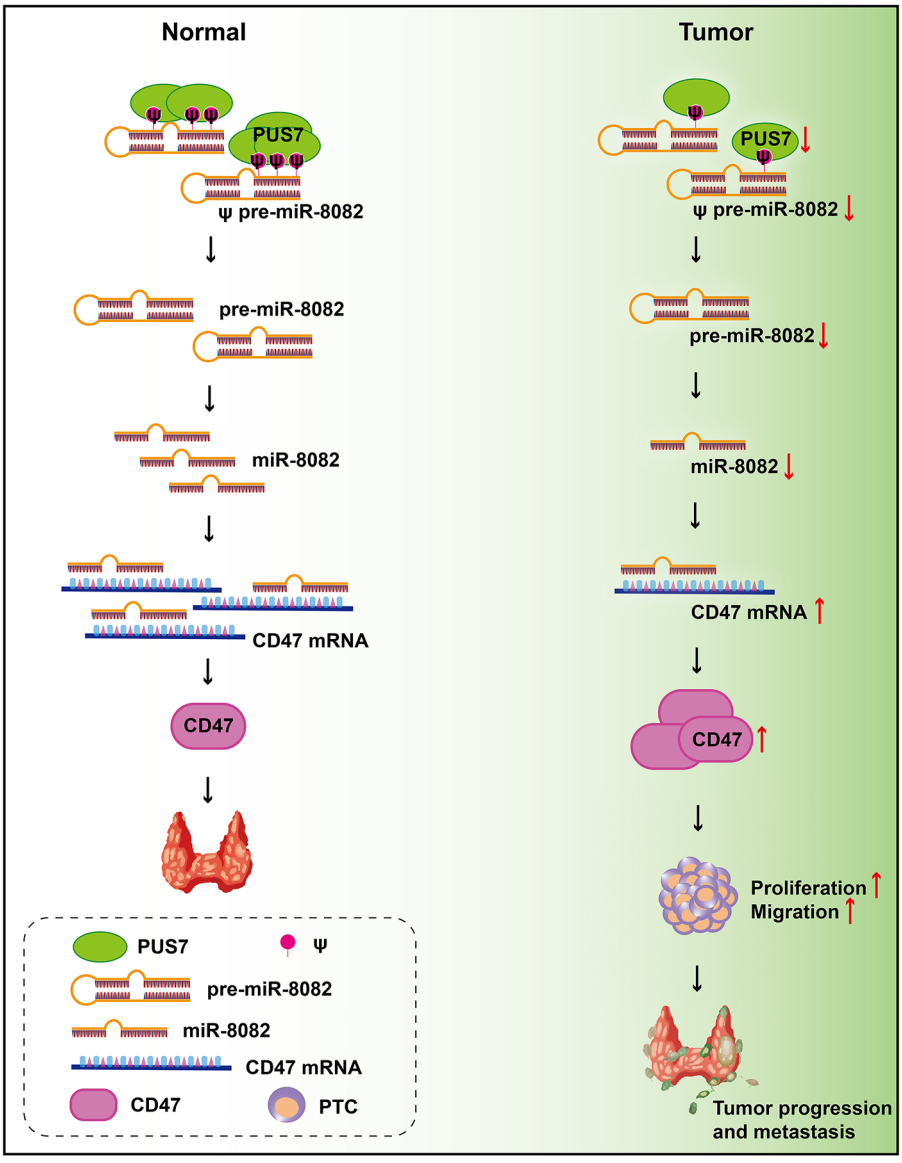

Fig. 7 Schematic illustrating the mechanism by which PUS7 promotes the inhibition of CD47 and suppresses the metastasis of PTC cells through the regulation of ψ modification of pre-miR-8082

can mediate the ψ modification of the pre-miR-8082, thereby affecting its maturation process. This modification will change the expression level of miR-8082 and further impact the expression of target genes. Our study found that a decrease in the level of ψ modification in the pre-miR-8082 precursor and an increase in miR-8082 expression in PTC selectively regulate the expression of CD47, a downstream target gene. CD47 is a significant transmembrane receptor molecule that is found to be overexpressed on the surface of several cancer cells [26]. It plays a role in anti-apoptosis, pro-proliferation, and pro-angiogenesis. CD47 binds to SIRPα on tumor cells, inhibiting macrophage phagocytosis in various cancers, including breast cancer, and leiomyosarcoma [27]. However, our findings suggest that the impact of CD47 is independent of macrophages in PTC. Furthermore, studies have indicated that CD47 expression is typically high in tumor cells, allowing them to evade immune system surveillance and attack [28]. Recent research has also demonstrated the involvement of CD47 in tumor metastasis [29]. CD47 not only affects the adhesion ability of tumor cells but also regulates signal transduction pathways in endothelial cells, thereby promoting tumor cell metastasis. CD47 may also collaborate with other molecules, such as Integrin β3 and TSP1, to form a complex signaling network that drives tumor cell metastasis [30]. In this study, we observed that inhibiting CD47 expression and disrupting tumor cell adhesion function prevented PTC metastasis. The precise

mechanism by which CD47 regulates PTC metastasis requires further investigation.

Conclusions

The study highlights the significance of abnormal levels of small RNA ψ modification in the metastasis of PTC. It demonstrates that PUS7 suppresses the migration of papillary thyroid carcinoma by repressing CD47 through pseudouridylated pre-miR-8082 (Fig. 7). Investigating the regulation of important small RNA modifications and their underlying mechanisms can help identify prognostic factors and potential drug targets with clinical relevance. This research improves our understanding of how small RNA ψ modification influences the development and spread of PTC. It guides selecting appropriate clinical treatment options, determining the extent of surgery, and managing the disease through various approaches.

Abbreviations

PUS7	pseudouridine synthase 7
PTC	papillary thyroid cancer
TSH	thyroid stimulating hormone
RAI	radioactive iodine
FNA	fine needle aspiration
ψ	pseudouridine
m1A	N1-methyladenosine
m6A	N6-methyladenosine
m7G	N7-methylguanosine
m5C	5-methylcytosine
DNMT1	DNA Methyltransferase 1
DNMT3A	DNA Methyltransferase 3 Alpha
DNMT3B	DNA Methyltransferase 3 Beta
METTL3	Methyltransferase 3
DEGs	differentially expressed genes
PI	propidium iodide
SOX4	SRY-Box Transcription Factor 4
CD47	CD47 Molecule
SLC16A7	Solute Carrier Family 16 Member 7
PSMB2	Proteasome 20 S Subunit Beta 2
CD74	CD74 Molecule
S100B	S100 Calcium Binding Protein B
GAS7	Growth Arrest Specific 7
SIPRα	signal regulatory proteinα
TSP1	Thrombospondin 1

Supplementary Information

The online version contains supplementary material available at https://doi.org/10.1186/s12935-024-03482-3.

Supplementary Material 1: Fig. 1. DNMT1, DNMT3B, METTL1, and METTL3 in PTC tissues. A-D. Correlation between the expression of DNMT1 (A), DNMT3B (B), METTL1 (C), and METTL3 (D) and relevant clinical characteristics (gender, pT stages, pN stages, pM stages, and pTNM stages). The high group refers to gene expression levels above the median expression, while the low group refers to gene expression levels below the median expression. E-F. Quantitative analysis of DNMT3B levels by qPCR (E) and IHC staining (F, data from HPA). Data are presented as Mean ± SD

Supplementary Material 2: Fig. 2. Enrichment of KEGG pathways and GO terms in the PUS7-high vs. PUS7-low groups of PTCs

Supplementary Material 3: Fig. 3. The top four differentially modified miRNAs and tsRNAs

Supplementary Material 4: Fig. 4. CD47 regulates tumor migration in a macrophage-independent way. (A) The macrophages infiltrated in PTCs with high and low CD47 expression. (B) Correlation of CD47 with the expression of marker genes of macrophage subtypes

Supplementary Material 5: Table 1. Primers for PCR

Supplementary Material 6: Table 2. Patients' background information

Supplementary Material 7: Table 3. Target genes of miR-8082 from TargetScan and miRDB databases

Acknowledgements

The authors would like to thank PTC patients who donated their specimens to the study.

Author contributions

Conceptualization, X.W. and H.Y.G; Investigation, X.W., H.Y.G., N.X., X.P.L., Z.P.Z. and W.J.P.; Writing-Original Draft, X.W. and H.Y.G.; Writing-Review & Editing, D.E.T. and Y.D.; Supervision, D.E.T. and Y.D.; Funding Acquisition, D.E.T. and Y.D. All authors read and approved the final manuscript.

Funding

This study was supported by the following funds: Shenzhen Science and Technology R&D Fund (JCYJ20190809165813331), Shenzhen Key Medical Discipline Construction Fund (SZXK059), the Science and Technology Plan of Shenzhen (JCYJ20180306140810282), and the Guangdong Provincial Enterprise Joint Foundation for Basic and Applied Basic Research General Project (No. 2023A1515220203).

Data availability

The datasets analyzed during the current study are not publicly available due to unpublished data being included but are available from the corresponding author upon reasonable request.

Declarations

Ethics approval and consent to participate

All patients enrolled in this study were informed, signed an informed consent form, and volunteered to participate. This project has been approved by the ethics committee of Shenzhen People's Hospital (LL-KY-2022091).

Consent for publication

Not applicable.

Competing interests

The authors declare no competing interests.

Received: 25 October 2023 / Accepted: 14 August 2024
Published online: 14 October 2024

References

1. Siegel RL, Miller KD, Jemal A. Cancer statistics, 2019. CA Cancer J Clin. 2019;69(1):7–34.
2. Megwalu UC, Moon PK. Thyroid Cancer Incidence and Mortality trends in the United States: 2000–2018. Thyroid. 2022;32(5):560–70.
3. Pu W, Shi X, Yu P, Zhang M, Liu Z, Tan L, Han P, Wang Y, Ji D, Gan H, et al. Single-cell transcriptomic analysis of the tumor ecosystems underlying initiation and progression of papillary thyroid carcinoma. Nat Commun. 2021;12(1):6058.
4. Luster M, Aktolun C, Amendoeira I, Barczynski M, Bible KC, Duntas LH, Elisei R, Handkiewicz-Junak D, Hoffmann M, Jarzab B, et al. European perspective on 2015 American Thyroid Association Management Guidelines for adult patients with thyroid nodules and differentiated thyroid Cancer: proceedings of an interactive International Symposium. Thyroid. 2019;29(1):7–26.
5. Tiedje V, Fagin JA. Therapeutic breakthroughs for metastatic thyroid cancer. Nat Rev Endocrinol. 2020;16(2):77–8.
6. Zhao Q, Ming J, Liu C, Shi L, Xu X, Nie X, Huang T. Multifocality and total tumor diameter predict central neck lymph node metastases in papillary thyroid microcarcinoma. Ann Surg Oncol. 2013;20(3):746–52.

7. Hwang HS, Orloff LA. Efficacy of preoperative neck ultrasound in the detection of cervical lymph node metastasis from thyroid cancer. Laryngoscope. 2011;121(3):487–91.
8. Yu J, Deng Y, Liu T, Zhou J, Jia X, Xiao T, Zhou S, Li J, Guo Y, Wang Y, et al. Lymph node metastasis prediction of papillary thyroid carcinoma based on transfer learning radiomics. Nat Commun. 2020;11(1):4807.
9. Sosa JA, Hanna JW, Robinson KA, Lanman RB. Increases in thyroid nodule fine-needle aspirations, operations, and diagnoses of thyroid cancer in the United States. Surgery. 2013;154(6):1420–6. discussion 1426–1427.
10. Roundtree IA, Evans ME, Pan T, He C. Dynamic RNA modifications in Gene expression regulation. Cell. 2017;169(7):1187–200.
11. Barbieri I, Kouzarides T. Role of RNA modifications in cancer. Nat Rev Cancer. 2020;20(6):303–22.
12. Janin M, Ortiz-Barahona V, de Moura MC, Martinez-Cardus A, Llinas-Arias P, Soler M, Nachmani D, Pelletier J, Schumann U, Calleja-Cervantes ME, et al. Epigenetic loss of RNA-methyltransferase NSUN5 in glioma targets ribosomes to drive a stress adaptive translational program. Acta Neuropathol. 2019;138(6):1053–74.
13. Blanco S, Bandiera R, Popis M, Hussain S, Lombard P, Aleksic J, Sajini A, Tanna H, Cortes-Garrido R, Gkatza N, et al. Stem cell function and stress response are controlled by protein synthesis. Nature. 2016;534(7607):335–40.
14. Cui Q, Shi H, Ye P, Li L, Qu Q, Sun G, Sun G, Lu Z, Huang Y, Yang CG, et al. M(6)a RNA methylation regulates the self-renewal and tumorigenesis of glioblastoma stem cells. Cell Rep. 2017;18(11):2622–34.
15. Su R, Dong L, Li C, Nachtergaele S, Wunderlich M, Qing Y, Deng X, Wang Y, Weng X, Hu C, et al. R-2HG exhibits anti-tumor activity by targeting FTO/m(6)A/MYC/CEBPA signaling. Cell. 2018;172(1–2):90–105. e123.
16. Fujita Y, Kuwano K, Ochiya T. Development of small RNA delivery systems for lung cancer therapy. Int J Mol Sci. 2015;16(3):5254–70.
17. Nombela P, Miguel-Lopez B, Blanco S. The role of m(6)A, m(5)C and psi RNA modifications in cancer: novel therapeutic opportunities. Mol Cancer. 2021;20(1):18.
18. Spenkuch F, Motorin Y, Helm M. Pseudouridine: still mysterious, but never a fake (uridine)! RNA Biol. 2014;11(12):1540–54.
19. Stockert JA, Gupta A, Herzog B, Yadav SS, Tewari AK, Yadav KK. Predictive value of pseudouridine in prostate cancer. Am J Clin Exp Urol. 2019;7(4):262–72.
20. Jiang T, Lin Y, Yin H, Wang S, Sun Q, Zhang P, Bi W. Correlation analysis of urine metabolites and clinical staging in patients with ovarian cancer. Int J Clin Exp Med. 2015;8(10):18165–71.
21. Sridharan G, Ramani P, Patankar S, Vijayaraghavan R. Evaluation of salivary metabolomics in oral leukoplakia and oral squamous cell carcinoma. J Oral Pathol Med. 2019;48(4):299–306.
22. Haran V, Lenka N. Deciphering the epitranscriptomic signatures in cell fate determination and development. Stem Cell Rev Rep. 2019;15(4):474–96.
23. Ali Syeda Z, Langden SSS, Munkhzul C, Lee M, Song SJ. Regulatory mechanism of MicroRNA expression in cancer. Int J Mol Sci 2020, 21(5).
24. Cui L, Ma R, Cai J, Guo C, Chen Z, Yao L, Wang Y, Fan R, Wang X, Shi Y. RNA modifications: importance in immune cell biology and related diseases. Signal Transduct Target Ther. 2022;7(1):334.
25. Matsuyama H, Suzuki HI. Systems and synthetic microRNA biology: from biogenesis to disease pathogenesis. Int J Mol Sci. 2019;21(1).
26. Kaur S, Isenberg JS, Roberts DD. CD47 (cluster of differentiation 47). Atlas Genet Cytogenet Oncol Haematol. 2021;25(2):83–102.
27. Zhang W, Huang Q, Xiao W, Zhao Y, Pi J, Xu H, Zhao H, Xu J, Evans CE, Jin H. Advances in anti-tumor treatments targeting the CD47/SIRPalpha axis. Front Immunol. 2020;11:18.
28. Myint ZW, Chahine Z, Jayswal R, Bachert E, McDonald RJ, Strup SE, James AC, Hensley PJ, Allison DB. Association of CD47 expression with clinicopathologic characteristics and survival outcomes in muscle invasive bladder Cancer. J Pers Med 2023, 13(6).
29. Qu S, Jiao Z, Lu G, Xu J, Yao B, Wang T, Wang J, Yao Y, Yan X, Wang T, et al. Human lung adenocarcinoma CD47 is upregulated by interferon-gamma and promotes tumor metastasis. Mol Ther Oncolytics. 2022;25:276–87.
30. Govatati S, Pichavaram P, Kumar R, Rao GN. Blockade of CD47 function attenuates restenosis by promoting smooth muscle cell efferocytosis and inhibiting their migration and proliferation. J Biol Chem. 2023;299(4):104594.

Publisher's note